Preliminary study of the splashing effect due to the bursting of giant water bubbles near the triple point: application to water evaporator

Florine Giraud, Patric Mantaropoulos, Brice Tremeac, Pascal Tobaly

DOI: 10.18462/iir. 10.18462/iir.icr.2023.0617

Preliminary study of the splashing effect due to the bursting of giant water bubbles near the triple point: application to water evaporator

Florine GIRAUD [a,b], Patric MANTAROPOULOS[a], Brice TREMEAC* [a], Pascal TOBALY[a,c]

[a] Lafset (Laboratoire du froid et des systèmes énergétiques et thermiques), Cnam, HESAM Université, 292 rue Saint-Martin 75003 Paris (France), brice.tremeac@lecnam.net

[b] LOCIE, Université Savoie Mont Blanc, CNRS UMR5271, Savoie Technolac, 73376 Le Bourget Du Lac, France, florine.giraud@univ-smb.fr

[c] Université Sorbonne Paris Nord, 99, av J.B. Clément, 93430 Villetaneuse, France

*Corresponding author: brice.tremeac@lecnam.net

ABSTRACT

Water offers various advantages in terms of environmental impact, thermophysical properties, cost and use. However, using water as refrigerant also has various drawbacks. To improve the fundamental knowledge about water vaporization at conditions representative of conditions obtained in the evaporator of a water refrigeration system, vaporization phenomena occurring inside a rectangular channel are studied. The impact of different parameters like the apparent surface of the bubble at the end of the growth, the location of the bubble at its early stage, and the channel thickness, in relation with the observed bubble behaviour, are discussed. It is shown that the height up to which the liquid is splashed (Δh_m^{max}) is highly related to the distance between the bubble at the beginning of the growth and the free interface (Δh_0) and that the latter parameter has an influence on the observed phenomena at the bubble scale.

Keywords: R-718, water, boiling, Evaporators, Energy Efficiency

1. INTRODUCTION

The use of water as a refrigerant in cooling systems is increasingly gaining interest since alternative to many commonly used refrigerants have to be found to cope with future environmental regulations. However, in water systems, boiling must take place at temperatures around 10 °C (corresponding to sub-atmospheric saturation pressures in the range of a few mbar) inside the evaporator. In these operating conditions, atypical bubble growth can be observed during water vaporisation. In particular, studies conducted in water pool-boiling conditions highlight mushroom-shaped bubbles with a diameter of several centimeters (Van Stralen *et al*. 1975, Michaie *et al.* 2019) and irregular cyclic regime (Mc Gillis *et al.* 1991, Giraud *et al.,* 2015). In a constrained environment (vertical rectangular channel partially filled with liquid), Giraud *et al.* (2019) highlight three main different phenomena at the top of the bubbles depending on the confinement number and depending on water vaporization production rate. They showed that at a confinement thickness of 2 mm, digitation develops at the bubble cap. A degradation of the overall heat transfer coefficient at low to middle superheat at this same confinement thickness was also recorded. Although bubble growth is a well-known phenomenon that has been studied and modelled since the middle of the 20th century, due to this complexity, commonly used models and correlations are not very effective in predicting phenomena and performances obtained at sub-atmospheric pressure (Sène et al.,2022). Simple models like Rayleigh model can predict the bubble growth of water at this low pressure and early stage but need to be adapted to the studied configuration. In addition, although the digitation phenomena have been studied at atmospheric pressure in Reinker et Kapitz (2016) and Kapitz *et al.* (2015) and in Mantaropoulos *et al.* (2023) in the present configuration, a lot of questions remain unanswered. Specially the impact of the observed phenomena on the heat transfer performance at the evaporator scale still in need to be studied. The aim of this paper is thus

to give some insight into the correlation between phenomena observed during the bubble growth and performance that could be expected at the evaporator scale.

2. EXPERIMENTAL SET-UP AND PREVIOUS MAJOR RESULTS

The experimental set-up used is the same as the one used in various publication including Giraud and Tremeac (2019) and Mantaropoulos *et al.* (2023). In order to understand the study discussed in this paper and its context, the experimental set-up is roughly introduced as well as previous major obtained results. More details are given in the referenced paper if needed.

2.1. Brief introduction of the experimental set-up

The studied evaporator is a smooth plate-type evaporator constituted of two narrow vertical channels, separated by a stainless-steel plate. The working fluid (distilled water) enters the first vertical channel by the bottom in a two-phase flow state. The secondary fluid (water) flows in the second channel in a co-current arrangement. The external wall of the first narrow vertical channel is made of PMMA to allow visualization (Fig. 1). The thickness of the channel can be adjusted to 2, 4 or 6 mm using a set of spacers. The second channel is 1mm thick. The secondary fluid flow rate is set to 1 L/min and its temperature is controlled using a thermostatic bath (B1 on figure 2). The working fluid flow rate is set between 1.79×10^{-3} L/min and 2.07×10^{-3} L/min.

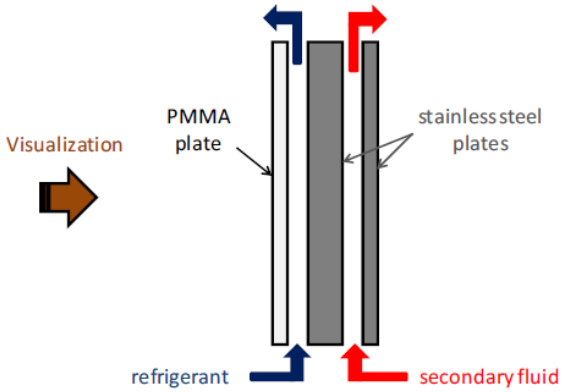

Figure 1: Schematic view of the test section (Giraud *et al.*, 2016)

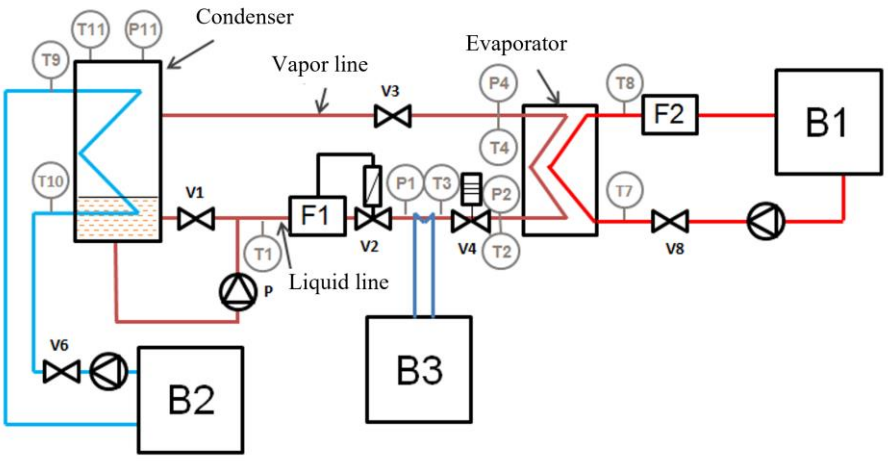

Figure 2: Schematic representation of the experimental set-up (Giraud *et al.*, 2016)

The working fluid vaporizes into the vertical channel thus created. Once vaporized it flows to a condenser constituted of a helicoidal heat-exchanger connected to a thermostatic bath (B2 in Fig. 1) and placed inside

a cylindrical tank. The fluid is stored in this tank before being expanded and flowing back inside the vertical channel.

T-type thermocouples and pressure transducers allow measuring the temperatures with an accuracy of ±0.1 K at the inlet and outlet of each component for the two fluids (primary and secondary) and the absolute pressure at different points of the test rig with an accuracy of ±0.075% of the reading. The coolant mass flow rate is measured using an electromagnetic flow meter with an accuracy of ±0.5% of the measured flow rate.

A high-speed camera (Phantom VEO410) is used to record images of the refrigerant at a frequency of 3000 to 5200 frames per second. The time increment between two images can be calculated with a precision of 10 μ s.

2.2. Previous major results

The experimental domain covered by experiments conducted with this experimental set-up is shown in Table 1. The liquid level refers to the distance from the bottom of the evaporator to the free surface.

Table 1. Experimental domain covered

Liquid level	Condenser secondary fluid temperature	Working pressure	Evaporator secondary fluid temperature	Narrow channel thickness
5 - 25 cm	2 – 15 °C	7-17 mBar	10 – 25 °C	2, 4 and 6mm

Some obtained results were already published and discussed in previous papers. In particular, obtained flow regimes (Giraud *et al*., 2016) and main phenomena observed at the bubble cap (Giraud and Tremeac*,* 2019) were described. As a background to fully understand the present paper, one should know:

- Three main heat transfer zones were observed (Giraud *et al.,* 2016): (i) A pool-boiling zone at the bottom of the heat-exchanger where bubbles and vapor masses are generated (the height of this pool boiling zone is the liquid level). Although bubbles are generated, the heat absorbed by the growth of these ones is negligible and the heat transferred in the whole liquid zone is almost null. (ii) A vapor zone at the upper part of the heat exchanger where, based on Nusselt number, the overall heat transfer coefficient is estimated to range around 11 $W.m^{-2}.K^{-1}$. (iii) A falling film zone located between the pool-boiling zone and the vapor zone where a liquid film created by the elevation of the free surface during large bubble growth and splashing effect due to the burst of bubbles (since the bubbles grow mostly upward and push the free surface up until it breaks) is observed. In this zone, heat transfer coefficients are estimated to range from 3 $kW.\ m^{-2}.K^{-1}$ up to 15 $kW.\ m^{-2}.K^{-1}$. Thus, the widest the liquid film zone the higher the heat-transfer performance (Fig. 3).

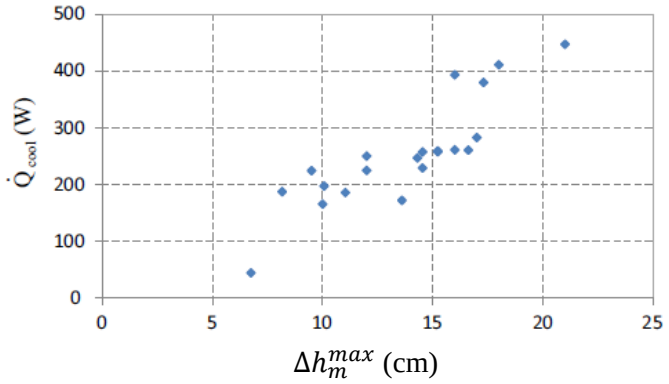

Figure 3: Evolution of the cooling capacity with the height of the liquid-film zone measured (Giraud *et al*., 2016)

- Three main phenomena at the bubble cap were observed during the growth of large bubbles (Giraud et Tremeac, 2019- Fig. 4): (i) smooth interface– no disturbance is observed; (ii) micro-boiling characterized by the occurrence of small bubbles probably located between the wall and the vapor encapsulated inside the bubble; (ii) fingering phenomena characterized by the formation of vapor fingers and detailed in Mantaropoulos *et al.* (2023).

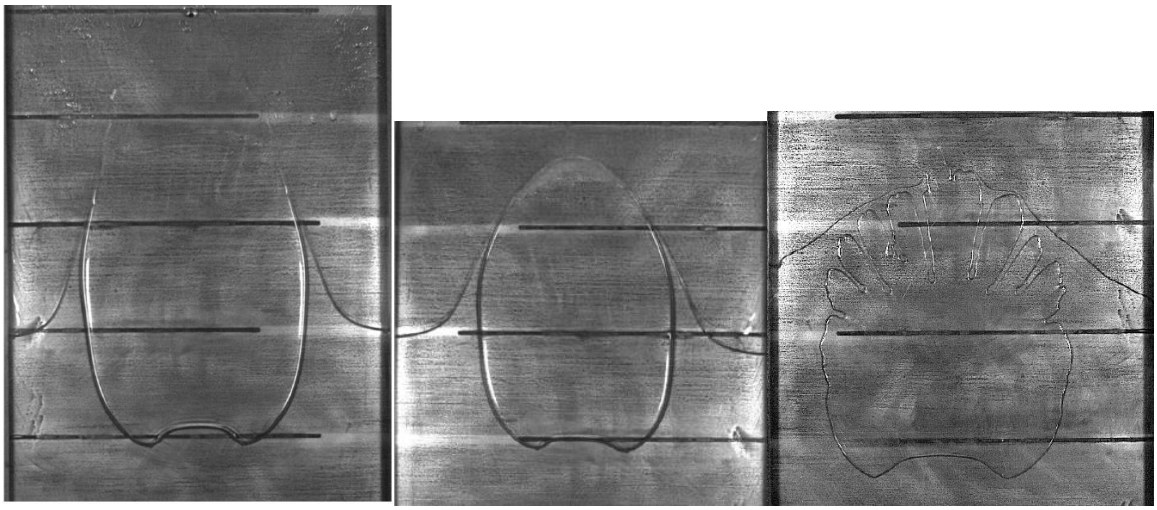

Figure 4: Main phenomena observed at the bubble cap (from left to right: smooth interface, micro-boiling and digitation)(Mantaropoulos, 2021)

3. EVOLUTION OF THE FILM ZONE AREA

Since it has been previously shown that the major part of the heat is transferred inside the film zone area, the objective of this section is to discuss the impact on the height of the film of the following parameters: the apparent surface of the bubble at the end of the growth, the location of the bubble at its early stage, the channel thickness and the inlet secondary fluid temperature, in relation with the observed bubble behaviour.

3.1. Calculation of the projection height

The film zone area corresponds to the area wetted by the working fluid due to an elevation of the free surface during the bubble growth and the projection of the droplets following the burst of the bubble. Since the image are automatically processed by a home-made Python program, the characteristic estimated is the height related to the deposited liquid film. It is calculated as the height difference between the free surface before the bubble apparition and the projection height (Fig. 5). The projection height is defined by the program as the maximum pixel density of the image above the free surface. The number of white pixels above the free surface is counted line by line and the altitude of the line containing the most pixels corresponds to a height in pixels, the reference being the bottom of the image.

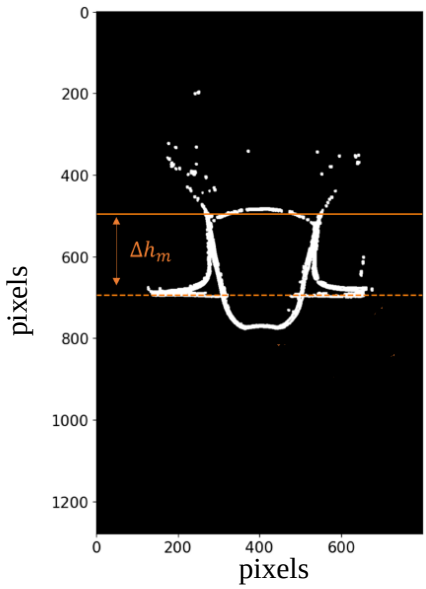

Figure 5: Example of processed image and illustration of the projection height calculated (Δh_m in pixels – modified from Mantaropoulos, 2021)

3.2. Evolution of the projection height with bubble geometrical characteristics

Fig. 6 shows the evolution of the maximal liquid film zone height with the apparent bubble area at burst time.

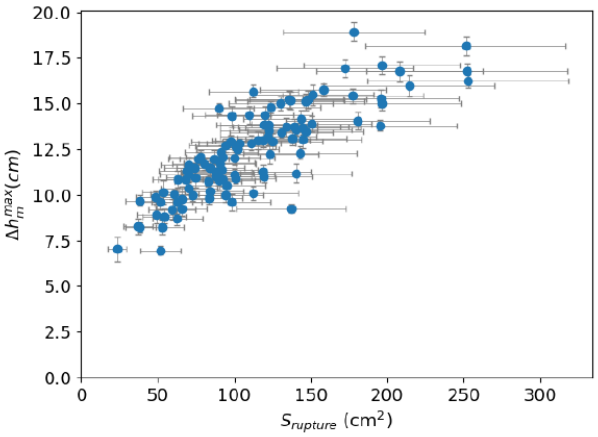

Figure 6: Evolution of the liquid zone height (Δh_m^{max}) with the apparent bubble area ($S_{rupture}$).

The general trend is an increase of the liquid film zone height with the increase of the apparent bubble size: for bubbles with an apparent area lower than 100 cm², a liquid film zone with a height lower than 12.5 cm is measured. On the other hand, liquid film height higher than 17.5 cm is measured for bubble of apparent area higher than 160 cm². This observation could be partly explained by two phenomena. First, the liquid film zone created by fluid displacement (Fig. 7a): the large bubble mostly grows upward (the foot of the bubble remains approximately at the same spot during the whole growth). The liquid displaced during its growth is thus mostly directed upward and around the bubble but weakly below the bubble foot. Thus, the larger the final bubble, the larger the amount of liquid displaced and the larger the liquid film area created by this liquid displacement (the liquid film zone height being calculated as the height difference between the free surface before the bubble apparition and the projection height). Second, according to Fig. 7b, large bubbles are more likely related to high bubble growth velocity at the time before the bursting. Thus, the energy related to the bubble growth could be transferred to the droplets at the time of the bursting and lead to greater projection height.

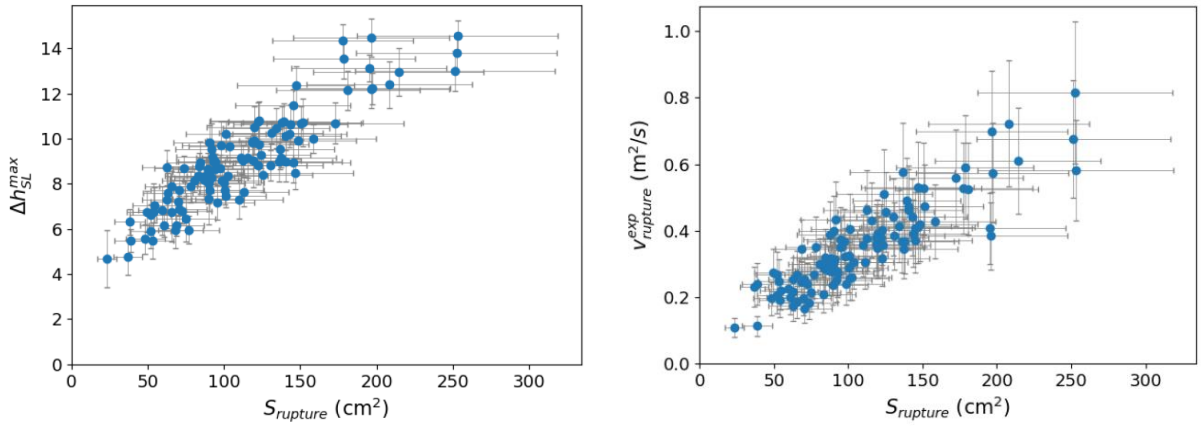

Figure 7: Evolution of a) the liquid displacement height (Δh_{SL}^{max}) and b) the bubble growth velocity ($V_{rupture}^{exp}$) with the apparent bubble area ($S_{rupture}$).

These two characteristics (bubble size and velocity at the end of the growth, just before the burst) are related to the distance between the spot where the bubble starts its growth and the free surface. The larger the distance between the nucleation site and the free surface, the larger the final bubble. This observation could be explained by the fact that the forces balance that drives the bubble growth is different when the bubble is deeply located inside the liquid medium (with solely a liquid-vapor interface, the vapor being inside the bubble) or partially exposed to the vapor medium (with, in the vapor medium, a double vapor-liquid-vapor interface). Further study should be conducted in order to determine the reason of the double interface vapor-liquid-vapor breaking (mechanical, thermal or both) and conclude about the bubble size at the burst time.

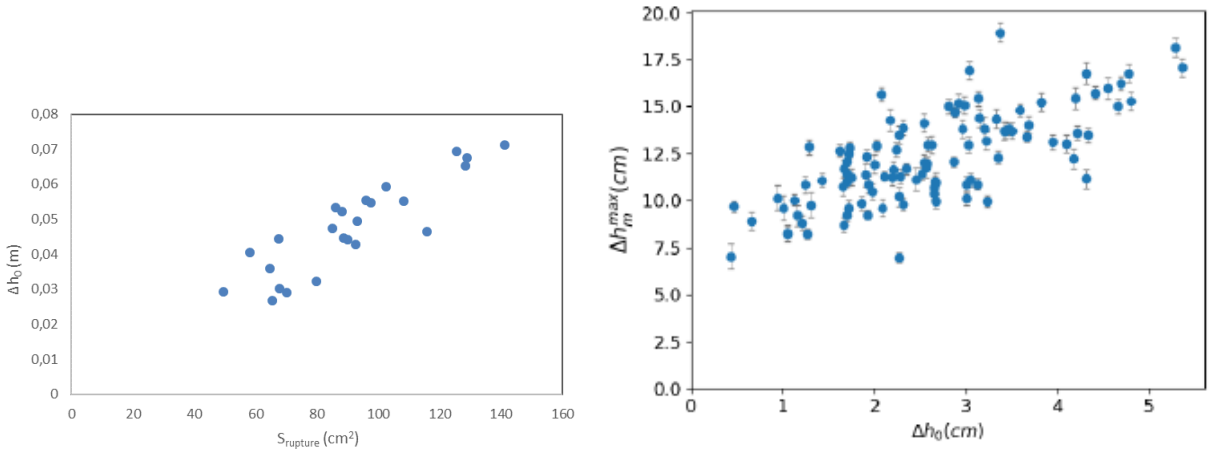

Figure 8: Evolution of a) the distance between the bubble at the beginning of the growth and the free interface (Δh_0) with the apparent bubble area ($S_{rupture}$) and b) the liquid zone height (Δh_m^{max}) with the apparent bubble Δh_0.

3.3. Evolution of the projection height with observed phenomena

In order to study the potential impact of observed phenomena on the liquid film zone height, the evolution of the latter with the apparent bubbles size for the different observed phenomena is plotted (Fig. 8). Since the case of micro-bubbles is difficult to discriminate, only fingering (or digitation) phenomena (only observed for e = 2 mm) and non-fingering phenomena (which could thus be micro-bubbles and smooth interface) is represented for the three thicknesses of the channel studied, i.e. 2 mm, 4 mm and 6 mm.

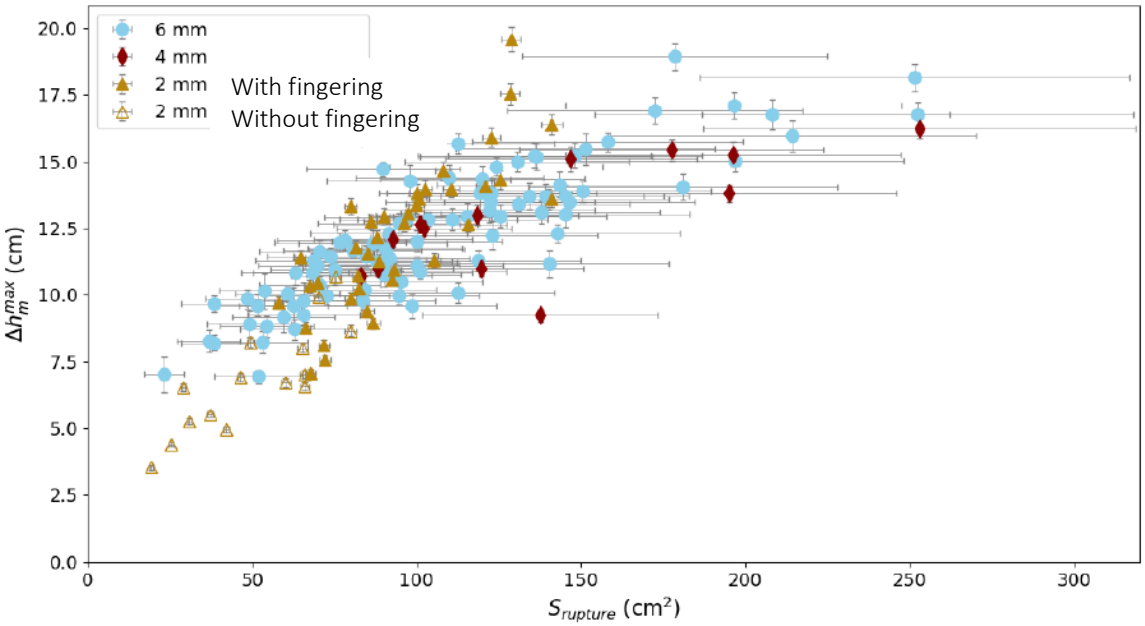

Figure 9: Evolution of the liquid zone height (Δh_m^{max}) with the apparent bubble area ($S_{rupture}$) for three channel thicknesses

According to Fig. 9, there is no significant impact of the channel thickness on the liquid zone height for a given bubble size. For bubble apparent area smaller than 50 cm², the lowest liquid zone height for a given bubble size seems likewise related to a channel thickness of 2 mm whereas at an apparent bubble size of around 130 cm², bubble obtained inside a channel 2 mm thick seems to lead to liquid zone height higher than 15 cm. This trend is similar to the trend observed in Giraud and Tremeac (2019) in term of enhancement factor: a thickness of 2 mm leads to the lowest but also highest performances depending on running conditions (more specifically, at high driving pressure, defined as the pressure difference between the saturation pressure corresponding to the superheated vapor inside the bubble assumed to be at the secondary fluid temperature and the vapor pressure - Eq.1 - a confinement of 2 mm leads to the highest performance whereas at low driving pressure it leads to the lowest performance). This improvement of performance for a thickness or the channel of 2 mm at high driving pressure was explained by Giraud and Tremeac by the observation of an upward liquid flow due to the high rate of vapor production obtained at these operating conditions. This observation could thus be an explanation for the high liquid zone height measured at middle apparent bubble sizes (around 130 cm²) for a 2 mm thick channel.

$$\Delta P = P_{sat}(T_{sc}) - P_{cond} \qquad \text{Eq. (1)}$$

Another interesting phenomenon observed in this Fig. 9, for 2 mm, is the location inside the graph of bubble with and without fingering: bubbles for which no fingering was observed for e = 2 mm are located on the bottom left of the graph. This observation could be also partly explained by the force balance on the bubble during its growth. It is clearly seen in Fig. 10 that the lower the nucleation depth, (i.e. the lower the distance between the free surface and the nucleation site), the lower the initial driving pressure (pressure difference between the inside and outside of the bubble) the more likely the stability of the bubble interface. A more in-depth study needs to be conducted in order to highlight phenomena leading to those instabilities.

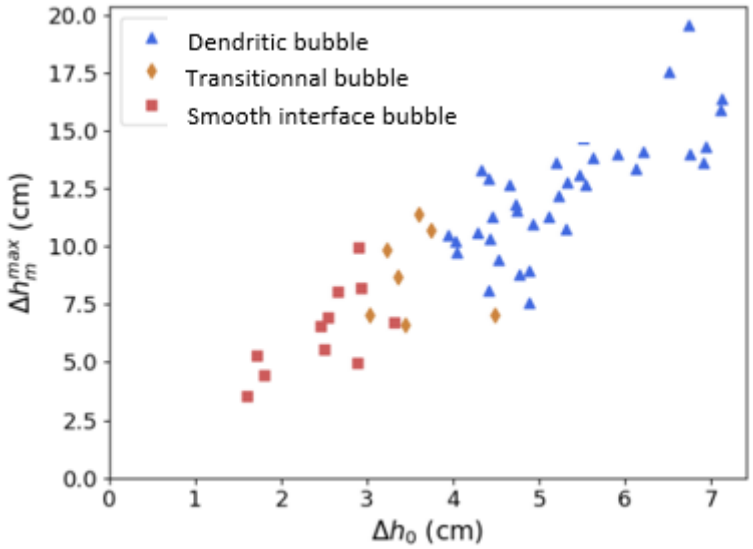

Figure 10: Evolution of the height up to which the liquid is splashed (Δh_m^{max}) versus the distance between the bubble at the beginning of the growth and the free interface (Δh_0) for different observed behaviours of bubbles (e = 2 mm)

4. TOWARDS THE DIMENSIONING OF LOW-PRESSURE EVAPORATOR

Based on these observations, dimensionless numbers are studied in order to be able to predict the film zone area. With this prediction, by using the correlations developed by Sène et al. (2022) or pool-boiling and falling film heat transfer coefficient, it is believed that the performance of the evaporator could be predicted.

Among the dimensionless numbers studied, Fig. 11 shows the evolution of the liquid film height with two interesting studied dimensionless number: Bond number and Ohnesorge Number. These two numbers are defined as follows:

$$Bo = \frac{g\Delta\rho {R_{max}^{eq}}^2}{\sigma} \quad \text{Eq. (2)}$$

$$Oh = \frac{\mu_l}{\sqrt{\rho_l \sigma R_{max}^{eq}}} \quad \text{Eq. (3)}$$

With R_{max}^{eq} the equivalent bubble radius leading to a disk surface of $S_{rupture}$, and μ_l, ρ, σ being respectively the liquid viscosity, the density and the surface tension.

The height of the liquid film zone increases with the Bond Number whereas it decreases with the Ohnesorge Number. These evolutions are consistent with Fig. 6 and Fig. 9 since the thermophysical properties of water slowly vary in comparison with the bubble size. It also gives an insight of the force balance by comparison of the buoyancy force compared to surface tension for Bo and viscous forces compared to surface tension for Oh. One may conclude that the buoyancy forces are highly predominant compare to surface tension and viscous forces since Bo range between 10^2-10^3 and Oh around 10^{-4}. Since the forces at work are probably mainly viscous, buoyancy, inertial and surface tension, this trend thus confirms that the bubble growth in these conditions is mainly governed by inertial effect and buoyancy forces. The Froude number is, indeed, close to 1 (Giraud and Tremeac, 2019). In addition, it seems that the higher the buoyancy force compared to the surface tension, the higher the liquid zone height and the higher the viscous force compared to the surface tension, the lower the liquid zone height.

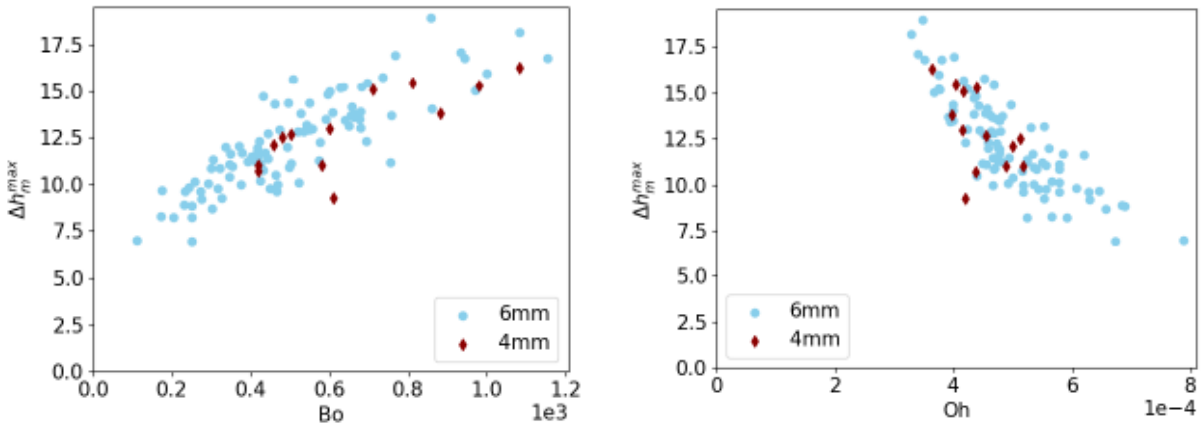

Figure 11: Evolution of the height up to which the liquid is splashed (Δh_m^{max}) versus a) the Bond Number and b) the Ohnesorge Number

5. CONCLUSIONS

Since it has been shown that the performance of a low-pressure smooth plate-type evaporator working with water as a working fluid is highly dependent on the liquid zone area created by the burst of bubbles, the impact of various parameters (at the bubble scale) on the created liquid film area is studied. In particular, the impact on the liquid zone height created by the burst of the bubble of the following parameters: bubble size at the time before the burst of a bubble, bubble growth velocity and the location of the nucleation site, is studied. It is shown that the larger the bubble at the time of the burst, the higher the liquid film zone area created. This is due to two mechanisms: the creation of a liquid film zone area by a liquid displacement during the bubble growth, and a wetted area created by projection of liquid droplets. Since it is also shown that the larger the bubble size, the more likely a high bubble growth velocity, this probably induces a higher projection height. Then the impact of the location of the nucleation site on these characteristics and on disturbances observed at the bubble cap are discussed. It is shown that the longer the distance between the nucleation site and the free surface, the larger the bubble and the more likely the observation of fingering for a channel 2 mm thick. These observations could probably be partly explained by the difference of forces at work when the bubble is fully immerged in a liquid medium (liquid-vapor interface) compared to forces at work in mix between a liquid and a vapor medium (double vapor-liquid-vapor interface in the vapor medium). Although, based on a dimensionless analysis in section 4, it is shown that the forces at work are mainly inertial and buoyancy forces at the time of the bubble growth, further work is required to, among-other, give a more in-depth study of the forces balance at (i) the time of the bubble growth, (ii) the bursting of the bubble; and be able to analyse if the burst is mainly driven by a mechanical or a thermal constraint.

NOMENCLATURE

g	Gravitational acceleration (m.s^{-2})	ρ	Density (kg/m3)
h	Height (m)	σ	Surface tension (N.m-1)
$\dot{Q}_{cool}$	Cooling capacity (W)	cond	Relative to the condenser
R	Radius (m)	exp	experimental
S	Area (m²)	l	Relative to the liquid
V	Velocity (m.s^{-1})	m	Total height
Δ	variation	max	maximal
μ	Dynamic Viscosity (N.s.m-2)	sat	saturation
0	Relative to the nucleation site	sc	Relative to the secondary fluid
		rupture	Relative to the burst of the bubble

REFERENCES

Giraud, F., Rullière, R., Toublanc, C., Clausse, M., & Bonjour, J. (2015). Experimental evidence of a new regime for boiling of water at subatmospheric pressure. *Experimental thermal and fluid science*, *60*, 45-53.

Giraud, F., Toublanc, C., Rullière, R., Bonjour, J., & Clausse, M. (2016). Experimental study of water vaporization occurring inside a channel of a smooth plate-type heat exchanger at subatmospheric pressure. *Applied Thermal Engineering*, *106*, 180-191.

Giraud, F., & Tremeac, B. (2019). Influences of confinement on subatmospheric water vaporization phenomena in a vertical rectangular channel. *International Journal of Heat and Mass Transfer*, *145*, 118725.

Kapitz, M., Reinker, F., & aus der Wiesche, S. (2015). Viscous fingering and heat transfer during boiling in a Hele–Shaw cell. *Experimental Thermal and Fluid Science*, *67*, 18-23.

Mantaropoulos, P. (2021). Vaporisation subatmosphérique de l'eau dans un canal vertical confiné: croissance de bulles, rupture d'interface et mouillage (Doctoral dissertation, Paris, HESAM).

Mantaropoulos, P., Giraud, F., Tréméac, B., & Tobaly, P. (2023). Dendritic bubble growth during the sub-atmospheric boiling of water in a narrow vertical channel. *Experimental Thermal and Fluid Science*, *141*, 110765.

McGillis, W. R., Carey, V. P., Fitch, J. S., & Hamburgen, W. R. (1991, February). Pool boiling enhancement techniques for water at low pressure. In *1991 Proceedings, Seventh IEEE Semiconductor Thermal Measurement and Management Symposium* (pp. 64-72). IEEE.

Michaie, S., Rullière, R., & Bonjour, J. (2019). Towards a more generalized understanding of pool boiling at low pressure: Bubble dynamics for two fluids in states of thermodynamic similarity. *Experimental Thermal and Fluid Science*, *101*, 217-230.

Reinker, F., & Kapitz, M. (2016). Boiling under hele-Shaw flow conditions: the occurrence of viscous fingering. *Journal of Heat Transfer*, *138*(2).

Sène, P., Giraud, F., Sow, M. L., & Tréméac, B. (2022). Heat transfer coefficient correlations of water subatmospheric vaporization in a channel of a smooth plate heat exchanger, based on Vaschy-Buckingham theorem. Applied Thermal Engineering, 118800.

Van Stralen, S. J. D., Cole, R., Sluyter, W. M., & Sohal, M. S. (1975). Bubble growth rates in nucleate boiling of water at subatmospheric pressures. *International Journal of Heat and Mass Transfer*, *18*(5), 655-669.